

Chiral Spin Liquid on a Kagome Antiferromagnet Induced by the Dzyaloshinskii-Moriya Interaction

Laura Messio,^{1,*} Samuel Bieri,² Claire Lhuillier,¹ and Bernard Bernu¹

¹*Laboratoire de Physique Théorique de la Matière Condensée, CNRS UMR 7600, Université Pierre et Marie Curie, Sorbonne Universités, 75252 Paris, France*

²*Institute for Theoretical Physics, ETH Zürich, 8099 Zürich, Switzerland*

(Received 6 January 2017; published 27 June 2017)

The quantum spin liquid material herbertsmithite is described by an antiferromagnetic Heisenberg model on the kagome lattice with a non-negligible Dzyaloshinskii-Moriya interaction (DMI). A well-established phase transition to the $\mathbf{q} = 0$ long-range order occurs in this model when the DMI strength increases, but the precise nature of a small-DMI phase remains controversial. Here, we describe a new phase obtained from Schwinger-boson mean-field theory that is stable at small DMI, and which can explain the dispersionless spectrum seen in the inelastic neutron scattering experiment by Han *et al.* [*Nature (London)* **492**, 406 (2012)]. It is a time-reversal symmetry breaking \mathbb{Z}_2 spin liquid, with the unique property of a small and constant spin gap in an extended region of the Brillouin zone. The phase diagram as a function of DMI and spin size is given, and dynamical spin structure factors are presented.

DOI: 10.1103/PhysRevLett.118.267201

Frustration in quantum magnets is a captivating and everlasting story. Competing interactions can lead to unconventional phases such as spin liquids (SL). After the first proposal by Anderson [1] of a quantum SL in the $S = 1/2$ Heisenberg model on the triangular lattice as a zero temperature disordered state, this notion has been greatly refined. A large number of such exotic phases have been discussed, notably on the antiferromagnetic kagome lattice, characterized by fractional symmetry quantum numbers [2,3].

Herbertsmithite is a paradigmatic material strongly suspected to host a SL. It was first synthesized in 2005 [4] and has since been subject to numerous experimental studies [5–12] (see [13] for a recent review). Herbertsmithite remains disordered down to very low temperatures, and it is described by an antiferromagnetic spin-1/2 Heisenberg model on the kagome lattice with strong nearest-neighbor interaction, $H_0 = J \sum_{\langle i,j \rangle} \mathbf{S}_i \cdot \mathbf{S}_j$, $J \approx 200$ K.

In view of the various proposed ground states, it appears that the low-energy physics is quite rich and that even small deformations of this idealized Hamiltonian can have crucial effects. Several perturbations are known to exist. Impurities are physically unavoidable [11] and theoretically challenging [14]. Here, we focus on the Dzyaloshinskii-Moriya interaction (DMI) [15–17]. Its value has been experimentally estimated to $D \approx 0.08J$ [8]. Theoretical studies [18–24] have concluded that a transition occurs between a small- D disordered phase and a $\mathbf{q} = 0$ Néel state at $D \gtrsim 0.1J$. But the precise nature of the disordered phase at small D is still unclear.

Here we describe a new chiral SL within the framework of Schwinger-boson mean-field theory (SBMFT) as a

strong candidate for the phase realized in herbertsmithite. The state has a unique property: the bottom of the spin excitation continuum is flat over an extended quasicircular region of the Brillouin zone. We compute the dynamical structure factor and confront it with data of Han *et al.* [10] and with the theory by Punk *et al.* [25].

Dzyaloshinskii-Moriya interaction.—The DMI [15,16] is a consequence of spin orbit coupling and comes from a broken mirror symmetry. It is characterized by vectors $\mathbf{D}_{ij} = 2J\theta_{ij}\mathbf{d}_{ij}$ on oriented links ($\mathbf{D}_{ij} = -\mathbf{D}_{ji}$), where $\mathbf{d}_{ij} = \mathbf{d}_{ji}$ has unit length. The total spin interaction on link (ij) is [17,26]

$$h_{ij} = JS'_i \cdot \mathbf{S}'_j, \quad (1)$$

where \mathbf{S}'_i and \mathbf{S}'_j are obtained from the original spins by rotations around the \mathbf{d}_{ij} axis with angles θ_{ij} and $-\theta_{ij}$, respectively. In the following, we set $J = 1$. The Hamiltonian is the sum over nearest-neighbor link energies,

$$H = \sum_{\langle i,j \rangle} h_{ij}. \quad (2)$$

When the composition of these rotations around a lattice loop is identity, then all nontrivial angles θ_{ij} can be removed by a unitary transformation and the spectrum is unaffected [29,30]. Otherwise, the effect of nonzero $\theta = |\theta_{ij}|$ depends on the geometry of the lattice. For example, on the antiferromagnetic square lattice, spins are unfrustrated and θ increases the ground state energy by introducing frustration. On the kagome lattice, the presence of loops with an odd number of sites (triangles) maximally frustrates antiferromagnetic interactions. In this case, a

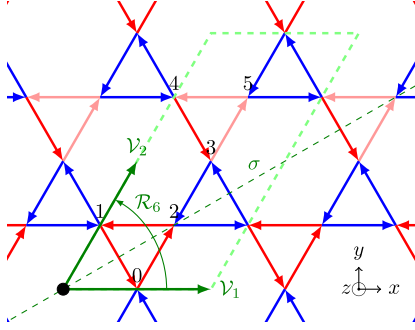


FIG. 1. The kagome lattice and its symmetries (in dark green). The orientation of the \mathbf{D}_{ij} (Dzyaloshinskii-Moriya) vectors on the directed links is out of plane. The unit cell of the *Ansatz* (light green) contains six sites. Red and blue arrows represent first-neighbor links wearing mean-field parameters \mathcal{A}_{ij} and \mathcal{B}_{ij} , equal to $|\mathcal{A}|$ and $|\mathcal{B}|e^{i\phi_B}$ on red links, and $|\mathcal{A}|e^{i\phi_A}$ and $|\mathcal{B}|e^{i(1-2p_R)\phi_B}$ on blue links, with an additional phase $p_1\pi$ on light red bonds.

nonzero θ decreases the ground state energy by reducing frustration.

Using crystal symmetry considerations, we can restrict the set of possible \mathbf{D}_{ij} . In herbertsmithite, it has constant modulus and is perpendicular to the (ij) link. Electron spin resonance measurements evaluated \mathbf{D}_{ij} to be mainly perpendicular to the kagome plane and of order $D = |\mathbf{D}_{ij}| \approx 0.08$ ($\theta \approx 0.04$) [8]. The direction of \mathbf{D}_{ij} on a reference link fixes all the other directions (Fig. 1). The tripartite nature of the lattice implies a $\pi/3$ periodicity in θ (up to a sublattice-dependent spin rotation). Since θ_{ij} and $-\theta_{ij}$ are equivalent up to a mirror reflection, we can limit our study to $0 \leq \theta \leq \pi/6$. The Hamiltonian of Eq. (2) breaks some symmetries of the pure Heisenberg model: σ (lattice mirror symmetry) and $SU(2)$ spin rotations. The preserved symmetries (Fig. 1) are generated by \mathcal{V}_1 and \mathcal{V}_2 (lattice translations), \mathcal{R}_6 (lattice rotation of order 6), $\sigma S_{\pi x}$ (mirror symmetry σ combined with a spin rotation of π around the x axis), $U(1)$ spin rotations around the z axis, and \mathcal{T} (time-reversal symmetry).

For classical spins, DMI immediately lifts the extensive ground state degeneracy of the Heisenberg model to the planar $\mathbf{q} = 0$ state of one of the two possible vector chiralities $\mathbf{S}_1 \wedge \mathbf{S}_2$ [18] [but the scalar chirality $\chi_{123} = \mathbf{S}_1 \cdot (\mathbf{S}_2 \wedge \mathbf{S}_3)$ remains zero]. In the quantum $S = 1/2$ model, a transition from a SL to this $\mathbf{q} = 0$ long-range order is expected at $D = D_c$, where $D_c \approx 0.1$ [19–21]. In the following, we elaborate on how to construct an elegant mean-field theory including DMI.

SBMFT and chiral phases.—In terms of the bosonic spinon $a_{i\alpha}$ of spin $\alpha \in \{\uparrow, \downarrow\}$ on site i , the spin operator reads as $\mathbf{S}_i = \frac{1}{2} a_{i\alpha}^\dagger \boldsymbol{\sigma}_{\alpha\beta} a_{i\beta}$, where $\boldsymbol{\sigma}$ are the Pauli matrices. The boson number is constrained to

$$\sum_{\alpha} a_{i\alpha}^\dagger a_{i\alpha} = 2S. \quad (3)$$

In the mean-field theory, this constraint is enforced on average with the help of a Lagrange multiplier λ .

We define two operators on each link (j, k) :

$$A_{jk} = \frac{1}{2} (e^{-i\theta_{jk}} a_{j\uparrow} a_{k\downarrow} - e^{i\theta_{jk}} a_{j\downarrow} a_{k\uparrow}), \quad (4)$$

$$B_{jk} = \frac{1}{2} (e^{i\theta_{jk}} a_{j\uparrow}^\dagger a_{k\uparrow} + e^{-i\theta_{jk}} a_{j\downarrow}^\dagger a_{k\downarrow}). \quad (5)$$

For $\theta = 0$, A_{jk} and B_{jk} are invariant under global spin rotation. For $\theta > 0$, this invariance is reduced to rotations around the z axis. The link interaction, Eq. (1), can be written as

$$h_{ij} = :B_{ij}^\dagger B_{ij}: - A_{ij}^\dagger A_{ij} \quad (6)$$

$$= S^2 - 2A_{ij}^\dagger A_{ij}, \quad (7)$$

where $::$ means normal ordering. Two different mean-field approximations can be developed using either the two parameters $\mathcal{A}_{ij} = \langle A_{ij} \rangle$ and $\mathcal{B}_{ij} = \langle B_{ij} \rangle$, and Eq. (6) (\mathcal{AB} formalism):

$$h_{ij}^{AB} = \mathcal{B}_{ij}^* \mathcal{B}_{ij} - \mathcal{A}_{ij}^* \mathcal{A}_{ij} + \text{H.c.} - |\mathcal{B}_{ij}|^2 + |\mathcal{A}_{ij}|^2, \quad (8)$$

or Eq. (7) and the parameter \mathcal{A}_{ij} only (\mathcal{A} formalism). Equations (6) and (7) are identical in spin space when the constraint Eq. (3) is exactly imposed. But in the enlarged Hilbert space of bosons where the constraint is only respected on average, they differ by a term $\propto (n_i - 2S)(n_j - 2S)$, related to the boson-number fluctuations. The \mathcal{A} formalism leads to inconsistencies, which have been discussed in detail for triangular and square lattices [31,32]. SBMFT has previously been used in attempts to describe DMI [20,21,33]. For the kagome lattice, however, this has only been done in the \mathcal{A} formalism so far.

In order to reduce the total number of link parameters, we use the notion of projective symmetry group [34,35]. This analysis has recently been extended to SLs where time reversal \mathcal{T} can be broken, but where lattice symmetries (or their composition with \mathcal{T}) are preserved [36–38]. Here, we restrict ourselves to *Ansätze* respecting the symmetries of Eq. (2) in this sense (Fig. 1). We thus consider the generators \mathcal{V}_1 , \mathcal{V}_2 , $\mathcal{T}^{p_R} \mathcal{R}_6$, and $\mathcal{T}^{p_\sigma} \sigma S_{\pi x}$, with $p_\sigma, p_R = 0$ or 1. This results in 20 *Ansatz* families listed in Table I. In all these cases, \mathcal{A}_{ij} and \mathcal{B}_{ij} on a reference link are propagated to the entire lattice by rules that depend on p_R and a parameter p_1 ($= 0$ or 1) related to the presence of an additional π flux through elementary tiles of the lattice. For each family, an *Ansatz* is characterized by two to four continuously adjustable parameters, corresponding to modulus and argument of \mathcal{A}_{ij} and \mathcal{B}_{ij} on the reference link, named $|\mathcal{A}|$, ϕ_A , $|\mathcal{B}|$, and ϕ_B . These parameters are adjusted until self-consistent saddle point solutions are found. In some families, ϕ_A and ϕ_B are restricted by discrete parameters p_A and/or p_B ($= 0$ or 1). The resulting

TABLE I. Description of the 20 *Ansatz* families respecting all symmetries of kagome with DMI, up to time reversal. p_R , p_σ , p_1 , p_A , and p_B (equal to 0 or 1) describe constraints on the link parameters and their propagation to the entire lattice (Fig. 1). “n.t.” means that the phase ϕ can take nontrivial values. The A_1 family has two adjustable parameters $|\mathcal{A}|$ and $|\mathcal{B}|$, whereas the others have three parameters (ϕ_A or ϕ_B in addition).

	p_R	p_σ	ϕ_A	ϕ_B
$A_1(p_1, p_A, p_B)$	0	0	$p_A\pi$	$p_B\pi$
$A_2(p_1, p_A)$	0	1	$p_A\pi$	n.t.
$A_3(p_1, p_A)$	1	0	$p_A\pi$	n.t.
$A_4(p_1, p_B)$	1	1	n.t.	$p_B\pi$

link parameters are described in Fig. 1 and in the last two columns of Table I.

Note that the families shown in Table I possess common *Ansätze*. Clearly, p_1 discriminates two *Ansätze* only when one of $|\mathcal{A}|$ or $|\mathcal{B}|$ is nonzero, while p_R and p_σ distinguish two *Ansätze* with identical p_1 only when ϕ_A or ϕ_B is nontrivial ($\neq 0$ or π). Some families can break \mathcal{T} due to nontrivial ϕ_A or ϕ_B . In this case, fluxes through lattice loops take nontrivial values leading to nonzero scalar spin chiralities. With Eq. (2), we do not find any self-consistent solution with $\phi_B \neq \pi$. As a result, the A_1 , A_2 , and A_3 families never break \mathcal{T} . Only a nontrivial ϕ_A (allowed in the families A_4) may break it.

On the kagome lattice, scalar chirality χ_{123} is usually associated with elementary triangles. In our framework, chiral *Ansätze* with $p_R = 0$ have uniform scalar chirality, while those with $p_R = 1$ have chiralities of the opposite sign on up and down triangles. This implies that a nonzero global (i.e., a macroscopic) chirality is only possible for $p_R = 0$. However, since χ_{123} is related to the imaginary part of $(|\mathcal{B}|e^{i\phi_B})^3$, this is always trivial since we find $\phi_B = \pi$. Thus, none of our solutions exhibit a macroscopic chirality.

In the following, we shall call *chiral state* any \mathcal{T} -breaking *Ansatz*, even in the absence of a macroscopic chirality. In such *Ansätze*, some χ_{123} are nonzero, e.g., for three consecutive sites of a hexagon. One could argue that the flux through a hexagon, $6\phi_B(1-p_R)+p_1\pi$ (phase of $\mathcal{B}_{12}\mathcal{B}_{23}\dots\mathcal{B}_{61}$), is still trivial. However, for loops with even parity, we can also consider the \mathcal{A} -flux $\arg[\mathcal{A}_{12}(-\mathcal{A}_{23}^*)\dots\mathcal{A}_{56}(-\mathcal{A}_{61}^*)]=3\phi_A+p_1\pi+\pi$. These two fluxes differ by their behavior under \mathcal{R}_6 rotation: the \mathcal{B} flux is invariant, while the \mathcal{A} flux changes sign. Thus, a nontrivial \mathcal{B} flux (only possible when $p_R = 0$) characterizes a uniform chirality, $\chi_{123} = \chi_{234}$, while a nontrivial \mathcal{A} flux (only possible when $p_R = 1$) characterizes a staggered chirality, $\chi_{123} = -\chi_{234}$. Note that, in the presence of a DMI, these fluxes contain θ in addition to the mean-field parameters, indicating a modified flux-chirality relation.

The existence of chiral phases as ground states [39–41] is already evident in the classical limit: an infinitesimal antiferromagnetic third-neighbor interaction lifts the

degeneracy of the kagome antiferromagnet to the nonplanar *cboc1* state [42]. In the \mathcal{AB} formalism, this phase melts into a stable chiral \mathbb{Z}_2 SL [family $A_4(1, 1)$ of Table I] at small spin [43]. This example of spontaneous generation of scalar chirality is a strong motivation for taking chiral *Ansätze* into account when solving the SBMFT problem with DMI.

Results.—We perform a numerical optimization of the parameters $|\mathcal{A}|$, $|\mathcal{B}|$, ϕ_A , and ϕ_B , using the injection of the measured parameters until convergence, combined with a Brent algorithm to optimize the phases. The mean-field energy is minimized with respect to $|\mathcal{A}|$ and ϕ_A , and maximized with respect to $|\mathcal{B}|$ and ϕ_B . The Lagrange multiplier λ is optimized each time a parameter is modified.

In SBMFT, the value of spin S is a continuous parameter, given by the average number of bosons per site [see Eq. (3)]. We optimize each *Ansatz* family in Table I, and we select the one with the lowest energy for fixed S and θ . So constructed phases either exhibit Néel order or are gapped (chiral) \mathbb{Z}_2 spin liquids [26]. Our results are summarized in Fig. 2 and discussed below. For completeness, we also reproduce the phase diagram of Ref. [20] in the \mathcal{A} formalism, but here we include time-reversal breaking states as well [Fig. 2(b)].

Let us discuss four special cases: $S \rightarrow \infty$, small S , $\theta = 0$, and $\theta = \pi/6$.

(a) $S \rightarrow \infty$: In the classical limit, we expect the mean-field solution to exhibit magnetic order through Bose-Einstein condensation of spinons. For $\theta = 0$, there is an extensive degeneracy, but the only Néel states that are reachable with our symmetric *Ansätze* are the *regular* ones, constructed in [42]. Three of them belong to the ground state manifold: $\mathbf{q} = 0$, $\sqrt{3} \times \sqrt{3}$, and *cboc1*. They are obtained, respectively, from $A_1(0, 0, 1)$, $A_1(0, 1, 1)$, and $A_4(1, 1)$ of Table I. All three *Ansätze* approach the same energy, and they show the classical values of the mean-field parameters [36]. A nonzero DMI favors $A_1(0, 0, 1)$ (i.e., $\mathbf{q} = 0$) consistent with a classical analysis.

(b) small S : In the \mathcal{A} formalism and following Tchernyshyov *et al.* [44], this limit can be solved through an expansion in S . In the presence of a DM flux,

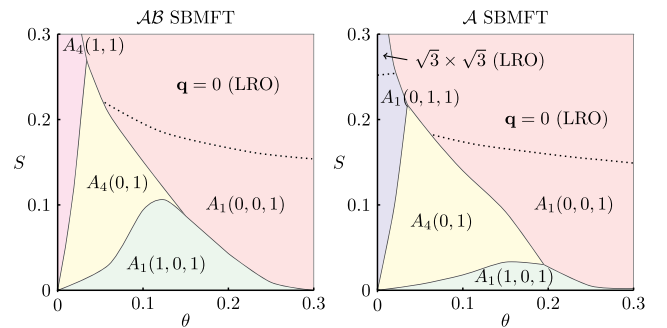


FIG. 2. Phase diagram. The *Ansatz* families with lowest self-consistent mean-field energy are indicated. LRO (above the dotted lines) means long-range order. The other phases are gapped \mathbb{Z}_2 SLs.

defined as the usual flux $\arg[\mathcal{A}_{ij}(-\mathcal{A}_{jk}^*) \dots \mathcal{A}_{lm}(-\mathcal{A}_{mi}^*)]$ plus $\theta_{ij} + \theta_{jk} + \dots + \theta_{mi}$, we find that the expansion of the energy to order 8 agrees with the right panel of Fig. 2, up to $S \approx 0.15$.

(c) $\theta = 0$ (pure Heisenberg case [45]): As shown previously [43], we find $A_4(1, 1)$ (i.e., *cuboc1*) in the \mathcal{AB} formalism and $A_1(0, 1, 1)$ (i.e., $\sqrt{3} \times \sqrt{3}$) in the \mathcal{A} formalism as the lowest-energy phase.

(d) $\theta = \pi/6$: Classically, the $\mathbf{q} = 0$ Néel state with well-chosen vector chirality minimizes the link energy and is the unique ground state. The Hamiltonian Eq. (2) is thus unfrustrated. It is equivalent to the XXZ model with ferromagnetic XX coupling. In this model, quantum Monte Carlo simulations found a superfluid phase [49]. As a consequence of the absence of frustration, $|\mathcal{B}| = 0$, and the two formalisms are equivalent (similar to the square lattice). $A_1(0, 0, 1)$ is thus the lowest-energy state for any value of spin (see Fig. 2).

Five of the 20 *Ansatz* families of Table I appear as ground states of our model in the range of parameters of Fig. 2. Two of them break \mathcal{T} and were absent in \mathcal{T} -symmetric investigations [20]. In addition to the chiral *Ansatz* $A_4(1, 1)$ already discussed for $\theta = 0$ [43], a new chiral phase is found here, both in the \mathcal{AB} formalism and in the \mathcal{A} formalism: the $A_4(0, 1)$ phase.

Since SBMFT contains unphysical boson number fluctuations, some care must be taken in the interpretation of these results [32]. However, we consistently obtain the new phase in two formalisms (\mathcal{A} and \mathcal{AB}), where the fluctuations are treated differently. This is an indication that the phase is robust and that it can survive an enforcement of the strict constraint Eq. (3).

The new chiral phase $A_4(0, 1)$ is separated from adjacent phases by first order phase transitions. Because of the hysteresis phenomenon, its domain of metastability is larger than shown in Fig. 2 [26]. It is notably metastable for $\theta = 0$ up to $S \approx 0.65$ in the \mathcal{AB} formalism, and up to $S \approx 0.3$ in the \mathcal{A} formalism. In its entire domain of metastability, this phase has a closed curve of minimal-energy spinons in the Brillouin zone (see Fig. 3). To our

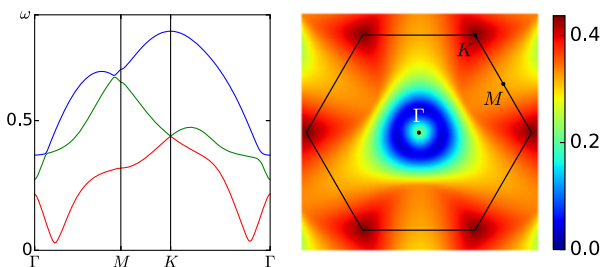


FIG. 3. Typical spinon spectra in the $A_4(0, 1)$ phase for small DMI and small spin (here $\theta = 0.01$ and $S = 0.5$; \mathcal{AB} formalism). The left panel shows the spinon energies along a cut; the right one shows the lowest band in the full Brillouin zone (with the characteristic ring of low-energy excitations).

knowledge, this intriguing property is unprecedented: previously studied gapped phases have sharply localized minima in the spinon spectrum [26].

Inelastic neutron scattering measures the dynamical structure factor $S(\mathbf{q}, \omega)$, i.e., the Fourier transformed space-time spin-spin correlations. In SBMFT, $S(\mathbf{q}, \omega)$ is nonzero when two spinons have the sum of their wave vectors equal to \mathbf{q} and of their energies equal to ω . In previously studied SLs, the low-lying spin excitations consist of combinations of a spinon at a singular spectral minimum with one in the low-energy branch. This leads to a high-intensity spot at the bottom of the excitation continuum, located at the Bragg peak of the corresponding classical phase, and to a strong dispersion away from this spot [50]. In contrast, for the new phase proposed in this Letter, any combination of two spinons on the minimum-energy curve has the same energy equal to twice the spinon gap. This leads to a spin excitation spectrum that is flat in an extended region of the Brillouin zone (Fig. 4).

Inelastic neutron data on single-crystal herbertsmithite revealed a surprising spreading of intensity over a wide range of wave vectors at very low energy ($0.75 \text{ meV} \approx 0.04J$) [10]. The low-energy structure factor of the $A_4(0, 1)$ phase, Fig. 4, indeed shows analogies with these results in the correct energy range, but with stronger intensity variations. The two bottom panels of Fig. 4 can be compared with Figs. 1(c) and 1(d) of [10], respectively.

An attempt to explain Han's results by including vison excitations in the $A_1(0, 0, 1)$ phase was realized by Punk *et al.* [25]. It was shown that this can indeed spread out the signal. But the energy scale of $A_1(0, 0, 1)$ was not naturally consistent with the experiment (theoretical results at $\omega = 0.37J$ were compared to an experimental cut at $\omega = 0.044J$). In the new $A_4(0, 1)$ phase, the energy scales are consistent, and we expect that adding vison excitations can give a fairly convincing agreement with experiment.

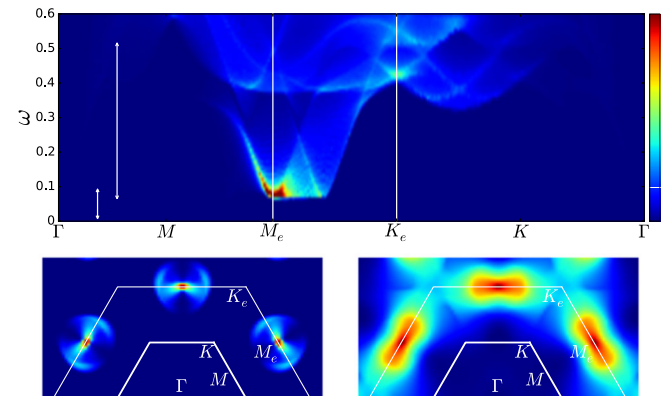


FIG. 4. Top: dynamical structure factor $S(\mathbf{q}, \omega)$ of the $A_4(0, 1)$ phase (same parameters as in Fig. 3). The spin gap is $0.06J$. Bottom left: $S(\mathbf{q}, \omega)$ integrated up to $\omega = 0.1J$. Bottom right: integrated over $0.06J < \omega < 0.52J$. See [26] for similar results using different model parameters.

Conclusion.—We have realized a SBMFT study of the kagome antiferromagnet with DMI, including time-reversal symmetry breaking *Ansätze*. One of the self-consistent solutions has particularly interesting features: it is a small-gap \mathbb{Z}_2 SL with a finite density of minimal-energy excitations, stable in an extended region of the phase diagram (Fig. 2). Its dynamical structure factor fairly well reproduces the inelastic neutron scattering measurements on herbertsmithite [10]: intensities around $\omega = 0.04J$ are obtained over a region of the Brillouin zone that is larger than in previously proposed \mathbb{Z}_2 SLs (Fig. 4). Inclusion of vison excitations [25] in the model will be a promising step towards a faithful correspondence between theory and experiment.

L.M. would like to thank K. Penc for interesting discussions on the DMI. This work was supported in part by Grant No. ANR-12-BS04-0021 (France).

*laura.messio@lptmc.jussieu.fr

- [1] P. W. Anderson, Resonating valence bonds: A new kind of insulator?, *Mater. Res. Bull.* **8**, 153 (1973).
- [2] Y. Qi and L. Fu, Detecting crystal symmetry fractionalization from the ground state: Application to \mathbb{Z}_2 spin liquids on the kagome lattice, *Phys. Rev. B* **91**, 100401 (2015).
- [3] M. Zaletel, Y.-M. Lu, and A. Vishwanath, Measuring space-group symmetry fractionalization in \mathbb{Z}_2 spin liquids, [arXiv:1501.01395](https://arxiv.org/abs/1501.01395).
- [4] M. P. Shores, E. A. Nytko, B. M. Bartlett, and D. G. Nocera, A structurally perfect $S = 1/2$ kagome antiferromagnet, *J. Am. Chem. Soc.* **127**, 13462 (2005).
- [5] M. Jeong, F. Bert, P. Mendels, F. Duc, J. C. Trombe, M. A. de Vries, and A. Harrison, Field-Induced Freezing of a Quantum Spin Liquid on the Kagome Lattice, *Phys. Rev. Lett.* **107**, 237201 (2011).
- [6] J. S. Helton, K. Matan, M. P. Shores, E. A. Nytko, B. M. Bartlett, Y. Yoshida, Y. Takano, A. Suslov, Y. Qiu, J.-H. Chung, D. G. Nocera, and Y. S. Lee, Spin Dynamics of the Spin-1/2 Kagome Lattice Antiferromagnet $\text{ZnCu}_3(\text{OH})_6\text{Cl}_2$, *Phys. Rev. Lett.* **98**, 107204 (2007).
- [7] P. Mendels, F. Bert, M. A. de Vries, A. Olariu, A. Harrison, F. Duc, J. C. Trombe, J. S. Lord, A. Amato, and C. Baines, Quantum Magnetism in the Paratacamite Family: Towards an Ideal Kagomé Lattice *Phys. Rev. Lett.* **98**, 077204 (2007).
- [8] A. Zorko, S. Nellutla, J. van Tol, L. C. Brunel, F. Bert, F. Duc, J.-C. Trombe, M. A. de Vries, A. Harrison, and P. Mendels, Dzyaloshinsky-Moriya Anisotropy in the Spin-1/2 Kagome Compound $\text{ZnCu}_3(\text{OH})_6\text{Cl}_2$, *Phys. Rev. Lett.* **101**, 026405 (2008).
- [9] M. A. de Vries, J. R. Stewart, P. P. Deen, J. O. Piatek, G. J. Nilsen, H. M. Rønnow, and A. Harrison, Scale-Free Antiferromagnetic Fluctuations in the $s = 1/2$ Kagome Antiferromagnet Herbertsmithite, *Phys. Rev. Lett.* **103**, 237201 (2009).
- [10] T.-H. Han, J. S. Helton, S. Chu, D. G. Nocera, J. A. Rodriguez-Rivera, C. Broholm, and Y. S. Lee, Fractionalized excitations in the spin-liquid state of a kagome-lattice antiferromagnet, *Nature (London)* **492**, 406 (2012).
- [11] T.-H. Han, M. R. Norman, J.-J. Wen, J. A. Rodriguez-Rivera, J. S. Helton, C. Broholm, and Y. S. Lee, Correlated impurities and intrinsic spin-liquid physics in the kagome material herbertsmithite, *Phys. Rev. B* **94**, 060409 (2016).
- [12] A. Zorko, M. Herak, M. Gomilšek, J. van Tol, M. Velázquez, P. Khuntia, F. Bert, and P. Mendels, Symmetry Reduction in the Quantum Kagome Antiferromagnet Herbertsmithite, *Phys. Rev. Lett.* **118**, 017202 (2017).
- [13] M. R. Norman, Colloquium : Herbertsmithite and the search for the quantum spin liquid, *Rev. Mod. Phys.* **88**, 041002 (2016).
- [14] I. Rousochatzakis, S. R. Manmana, A. M. Läuchli, B. Normand, and F. Mila, Dzyaloshinskii-Moriya anisotropy and nonmagnetic impurities in the $s = \frac{1}{2}$ kagome system $\text{ZnCu}_3(\text{OH})_6\text{Cl}_2$, *Phys. Rev. B* **79**, 214415 (2009).
- [15] I. E. Dzyaloshinskii, A thermodynamic theory of weak ferromagnetism of antiferromagnetics, *J. Phys. Chem. Solids* **4**, 241 (1958).
- [16] T. Moriya, Anisotropic Superexchange Interaction and Weak Ferromagnetism, *Phys. Rev.* **120**, 91 (1960).
- [17] L. Shekhtman, O. Entin-Wohlman, and A. Aharony, Moriya's Anisotropic Superexchange Interaction, Frustration, and Dzyaloshinsky's Weak Ferromagnetism, *Phys. Rev. Lett.* **69**, 836 (1992).
- [18] M. Elhajal, B. Canals, and C. Lacroix, Symmetry breaking due to Dzyaloshinsky-Moriya interactions in the kagome lattice, *Phys. Rev. B* **66**, 014422 (2002).
- [19] O. Cépas, C. M. Fong, P. W. Leung, and C. Lhuillier, Quantum phase transition induced by Dzyaloshinskii-Moriya interactions in the kagome antiferromagnet, *Phys. Rev. B* **78**, 140405 (2008).
- [20] L. Messio, O. Cépas, and C. Lhuillier, Schwinger-boson approach to the kagome antiferromagnet with Dzyaloshinskii-Moriya interactions: Phase diagram and dynamical structure factors, *Phys. Rev. B* **81**, 064428 (2010).
- [21] Y. Huh, L. Fritz, and S. Sachdev, Quantum criticality of the kagome antiferromagnet with Dzyaloshinskii-Moriya interactions, *Phys. Rev. B* **81**, 144432 (2010).
- [22] M. Rigol and R. R. P. Singh, Magnetic Susceptibility of the Kagome Antiferromagnet $\text{ZnCu}_3(\text{OH})_6\text{Cl}_2$, *Phys. Rev. Lett.* **98**, 207204 (2007).
- [23] T. Dodds, S. Bhattacharjee, and Y. B. Kim, Quantum spin liquids in the absence of spin-rotation symmetry: Application to herbertsmithite, *Phys. Rev. B* **88**, 224413 (2013).
- [24] M. Hering and J. Reuther, Functional renormalization group analysis of Dzyaloshinsky-Moriya and Heisenberg spin interactions on the kagome lattice, *Phys. Rev. B* **95**, 054418 (2017).
- [25] M. Punk, D. Chowdhury, and S. Sachdev, Topological excitations and the dynamic structure factor of spin liquids on the kagome lattice, *Nat. Phys.* **10**, 289 (2014).
- [26] See Supplemental Material at <http://link.aps.org/supplemental/10.1103/PhysRevLett.118.267201> for further details on spectral properties, comparison with experiment, and the theory of DMI and SMBFT, which includes Refs. [27,28].
- [27] S. Sachdev, Kagome- and triangular-lattice Heisenberg antiferromagnets: Ordering from quantum fluctuations

- and quantum-disordered ground states with unconfined bosonic spinons, *Phys. Rev. B* **45**, 12377 (1992).
- [28] N. Read and S. Sachdev, Large- N Expansion for Frustrated Quantum Antiferromagnets, *Phys. Rev. Lett.* **66**, 1773 (1991).
- [29] T. A. Kaplan, Single-band Hubbard model with spin-orbit coupling *Z. Phys. B* **49**, 313 (1983).
- [30] K. Essafi, O. Benton, and L. Jaubert, A kagome map of spin liquids from XXZ to Dzyaloshinskii-Moriya ferromagnet *Nat. Commun.* **7**, 10297 (2016).
- [31] R. Flint and P. Coleman, Symplectic N and time reversal in frustrated magnetism, *Phys. Rev. B* **79**, 014424 (2009).
- [32] A. Mezio, C. N. Sposetti, L. O. Manuel, and A. E. Trumper, A test of the bosonic spinon theory for the triangular antiferromagnet spectrum, *Europhys. Lett.* **94**, 47001 (2011).
- [33] L. O. Manuel, C. J. Gazza, A. E. Trumper, and H. A. Ceccatto, Heisenberg model with Dzyaloshinskii-Moriya interaction: A Schwinger boson study, *Phys. Rev. B* **54**, 12946 (1996).
- [34] X.-G. Wen, Quantum orders and symmetric spin liquids, *Phys. Rev. B* **65**, 165113 (2002).
- [35] F. Wang and A. Vishwanath, Spin-liquid states on the triangular and Kagomé lattices: A projective-symmetry-group analysis of Schwinger boson states, *Phys. Rev. B* **74**, 174423 (2006).
- [36] L. Messio, C. Lhuillier, and G. Misguich, Time-reversal-symmetry-breaking chiral spin liquids: a projective symmetry group approach of bosonic mean-field theories, *Phys. Rev. B* **87**, 125127 (2013).
- [37] S. Bieri, L. Messio, B. Bernu, and C. Lhuillier, Gapless chiral spin liquid in a kagome Heisenberg model, *Phys. Rev. B* **92**, 060407 (2015).
- [38] S. Bieri, C. Lhuillier, and L. Messio, Projective symmetry group classification of chiral spin liquids, *Phys. Rev. B* **93**, 094437 (2016).
- [39] X.-G. Wen, F. Wilczek, and A. Zee, Chiral spin states and superconductivity, *Phys. Rev. B* **39**, 11413 (1989).
- [40] K. Yang, L. K. Warman, and S. M. Girvin, Possible spin-liquid states on the triangular and kagomé lattices, *Phys. Rev. Lett.* **70**, 2641 (1993).
- [41] W.-J. Hu, W. Zhu, Y. Zhang, S. Gong, F. Becca, and D. N. Sheng, Variational Monte Carlo study of a chiral spin liquid in the extended Heisenberg model on the kagome lattice, *Phys. Rev. B* **91**, 041124 (2015).
- [42] L. Messio, C. Lhuillier, and G. Misguich, Lattice symmetries and regular magnetic orders in classical frustrated antiferromagnets, *Phys. Rev. B* **83**, 184401 (2011).
- [43] L. Messio, B. Bernu, and C. Lhuillier, Kagome Antiferromagnet: A Chiral Topological Spin Liquid?, *Phys. Rev. Lett.* **108**, 207204 (2012).
- [44] O. Tchernyshyov, R. Moessner, and S. L. Sondhi, Flux expulsion and greedy bosons: Frustrated magnets at large N , *Europhys. Lett.* **73**, 278 (2006).
- [45] The presence of a gap in the pure Heisenberg spin liquid remains controversial. Recent approaches weigh in at a gapless state [46–48].
- [46] H. J. Liao, Z. Y. Xie, J. Chen, Z. Y. Liu, H. D. Xie, R. Z. Huang, B. Normand, and T. Xiang, Gapless Spin-Liquid Ground State in the $S = 1/2$ Kagome Antiferromagnet, *Phys. Rev. Lett.* **118**, 137202 (2017).
- [47] Y.-C. He, M. P. Zaletel, M. Oshikawa, and F. Pollmann, Signatures of Dirac cones in a DMRG study of the Kagome Heisenberg model, [arXiv:1611.06238](https://arxiv.org/abs/1611.06238).
- [48] Y. Iqbal, F. Becca, S. Sorella, and D. Poilblanc, Gapless spin-liquid phase in the kagome spin- $\frac{1}{2}$ Heisenberg antiferromagnet, *Phys. Rev. B* **87**, 060405 (2013).
- [49] S. V. Isakov, S. Wessel, R. G. Melko, K. Sengupta, and Y. B. Kim, Valence Bond Solids and Their Quantum Melting in Hard-Core Bosons on the Kagome Lattice, *Phys. Rev. Lett.* **97**, 147202 (2006).
- [50] J. C. Halimeh and M. Punk, Spin structure factors of chiral quantum spin liquids on the kagome lattice, *Phys. Rev. B* **94**, 104413 (2016).